Geochemical Perspectives Letters

The magma ocean was a huge helium reservoir in the early Earth

O. Ozgurel[1*], R. Caracas[1,2]

https://doi.org/10.7185/geochemlet.2314

Abstract

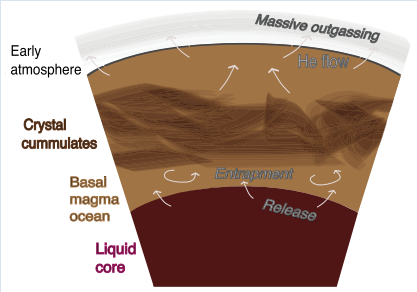

Helium from mantle-derived rocks bears in its isotopic ratios the traces of Earth differentiation, degassing, and long term geodynamic evolution. The low ^{4}He/^{3}He ratio of rocks whose origins are in the deep mantle, like ocean island basalts (OIBs), reflect potentially concealed geochemical reservoirs rich in primordial ^{3}He and isolated from the surface. Here we search for the geological repository of primordial He lasting from the core formation. For this, we determine the chemical behaviour of He in the magma ocean (MO) during core formation. We perform *ab initio* molecular dynamics simulations at temperatures and pressures along the MO adiabat. Our results show that primordial He was largely trapped in MO. At the top, under the hot dense early atmosphere, He remained mainly in the MO and degassed only later, at low atmospheric pressure. At the bottom, He partitions preferentially into the MO rather than the liquid core. The origin of the OIBs reflects a large contribution and contamination from mantle sources and no contribution from the top of the outer core, depleted in primordial He. We suggest the search for the He reservoirs should be done at the base of the solid mantle.

Received 23 November 2022 | Accepted 21 March 2023 | Published 10 May 2023

Introduction

Noble gases are useful geochemical tracers of physical processes. Their non-radiogenic isotopes are residues of the Big Bang or of stellar nucleosynthesis. They were accreted from nebular gases, from meteoritic material irradiated by solar wind, and/or delivered by chondritic or cometary material (Marty, 2012; Moreira, 2013). They were largely degassed from the mantle during the partial or total melting episodes of the early Earth. Whatever fraction remained, was stored in geochemical reservoir(s) inside the Earth, from where they continuously escape at a slow rate *via* deep melts that eventually bring them to the surface. Their concentration in deep Earth reservoirs, therefore, decreases over geological time. The radiogenic isotopes of noble gases are products of nuclear decay reactions from unstable parent isotopes, like ^{238}U, ^{235}U, or ^{232}Th, which are lithophile elements (Bouhifd *et al.*, 2013). The radiogenic noble gas isotopes are therefore replenished over geological time. Their ratios of non-radiogenic to radiogenic isotopes arriving at the surface constrain the isolation and mixing of Earth's internal reservoirs over geological time (Marty, 2012; Moreira, 2013; Jackson *et al.*, 2017; Péron *et al.*, 2018).

In particular, He received decades of attention from the Earth and planetary community. The degassed He from the crust and mantle continuously escapes into space from the Earth's atmosphere, unlike much heavier noble gases. As He is not recycled back into the mantle in important quantities, its radiogenic ^{4}He to primordial ^{3}He isotopic ratio preserves ancient MO signatures. One such signature is the low ^{4}He/^{3}He ratio observed in ocean island basalts (OIBs) such as Iceland, Hawaii, the Galapagos, Reunion and Samoa, which are the surface manifestations of deep mantle plumes (*e.g.*, Farley *et al.*, 1992; Kurz and Geist, 1999; Stuart *et al.*, 2003). They sample a significantly low degassed deep reservoir, which has preserved most of its ^{3}He. The mid-ocean ridge basalts (MORBs) bear a significantly different signature with a comparatively higher ^{4}He/^{3}He ratio. Their origin is in the more degassed upper mantle (Trieloff and Kunz, 2005; Moreira, 2013; Jackson *et al.*, 2017; Péron *et al.*, 2018; Mukhopadhyay and Parai, 2019). Whole mantle convection models show that there are only a few possible isolated places in the mantle today, like the D″ layer (Tolstikhin and Hofmann, 2005) or the large low shear wave velocity provinces (LLSVPs; Jackson and Carlson, 2011), which could still be largely undegassed. Another hypothesis to explain the high primordial He ratio in OIBs is the isolation of the plume source from the MORB source for more than 1 Gyr (Class and Goldstein, 2005). The alternative possibility is that the noble gas reservoirs are hidden in the Earth's core (Matsuda *et al.*, 1993; Bouhifd *et al.*, 2013; Jackson *et al.*, 2017; Olson and Sharp, 2022). A series of recent computational studies (Xiong *et al.*, 2021; Yuan and Steinle-Neumann, 2021; Wang *et al.*, 2022) proposed the same origin, although they found out that noble gases partition preferentially in the silicate melt, *i.e.* into the MO.

The first condition to store primordial He in a mantle reservoir is preferential He partitioning into the MO in the early Earth. The second condition is to trap He in the MO by preventing degassing into the atmosphere. Here we investigate these two aspects. We study from *ab initio* molecular dynamics simulations the chemical behaviour of He at the two boundaries of the MO: at the base, at the contact with the molten liquid core and at the top, at the contact with the atmosphere. Moreover,

1. The Center for Earth Evolution and Dynamics, University of Oslo, 0371 Oslo, Norway
2. Université de Paris, Institute de Physique du Globe de Paris, CNRS, 1 Rue Jussieu, 75005 Paris, France
* Corresponding author (email: ozge.ozgurel@geo.uio.no)

instead of using simplified Mg silicate models for the MO, we employ the bulk silicate Earth model (McDonough and Sun, 1995) to approximate the global MO, which we call *pyrolite*. In our simulations, first we decrease the density of He-bearing pyrolite until we reach the liquid-vapour dome. We perform a detailed analysis of the interatomic connectivity in the simulation cell; we identify free atoms and molecules that occupy void spaces and constitute the gas phase. Second we put in contact pyrolite and iron melts, allow them to equilibrate, and perform long production simulations where the He atoms are allowed to migrate between the two melts. All the computational details are given in the Supplementary Information.

Degassing into the Hot Dense Early Atmosphere

The top of the MO was in contact with a dense hot atmosphere, which dominated the early Earth. Until the formation of the first crust, which protected the liquid silicate from the atmosphere, the flux of volatiles degassing from the MO was rich in CO_2 and poor in H_2O (Solomatova and Caracas, 2021). The results of our degassing simulations suggest that He follows a devolatilisation trend with pressure that is similar to that of CO_2. At pressures above 1 GPa, corresponding in our simulations to magma densities in the range 2.5–3.6 g/cm^3, all of the He is dissolved in the silicate melt, without any formation of gas bubbles. These densities are similar to ultramafic lavas at present day surface conditions. As we decrease the melt density below 2.0 g/cm^3, cavities with volatiles start to form. As a result, the system now consists of polymerised pyrolite melt and a vapour-like phase composed of volatile atoms and atomic clusters. The ratio between the concentration of He inside the pyrolite melt and the gaseous phase enables us to quantify the He vapourisation as a function of density and temperature (Fig. 1).

He degassing starts below 2.0 g/cm^3. Down to about 1.6 g/cm^3, the devolatilisation is less than 10 %. At these conditions, the rate and amount of degassing is weakly dependent on He concentration and temperature. Below 1.6 g/cm^3, the opening of the silicate framework that is the backbone of the melt allows for massive devolatilisation, similar to CO_2 degassing from pyrolite (Solomatova and Caracas, 2021). He degassing is favoured by the increase in the amount of total He present in the system. At the lowest density examined in this study (1.1 g/cm^3), about 50 % (±10 %) of He exists in the vapour phase for the low concentration system (pyrolite + 0.25 wt. % He). At higher concentrations (pyrolite + 1.0 wt. % He), He volatility does not change significantly within the resolution of this study.

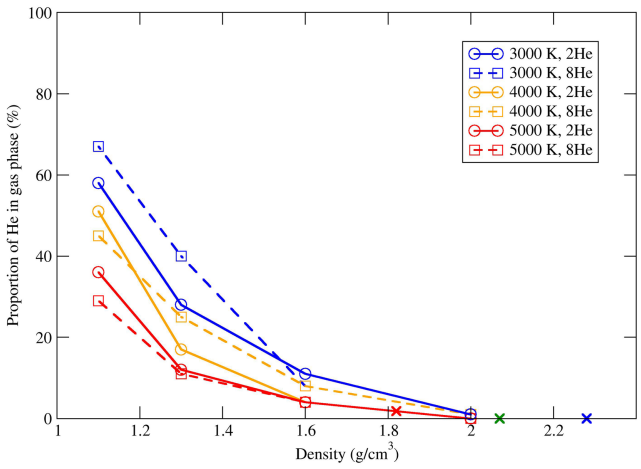

Figure 1 Proportion of He in the gas phase relative to molten pyrolite. 1 kbar approximately corresponds to a melt-vapour system density of 2.3, 2.1 and 1.8 g/cm^3 at 3000, 4000 and 5000 K, respectively ("×" symbols).

To express He vapourisation as a function of temperature along isobars, we fit our density values to a third order Birch-Murnaghan equation of state in the pressure range 1 to 10 kbar (Fig. S-6). At these conditions, He concentration in pyrolite is in the range 2400–2500 ppm, in good agreement with concentrations calculated in molten CI chondrites below 8 GPa (Bouhifd *et al.*, 2013). At constant pressure, the He volatility increases with increasing temperature. Nevertheless, He remains mostly dissolved in the silicate melt at surface pressures analogous to the early MO covered by a thick dense atmosphere. As the atmospheric pressure decreases, the degassing accelerates and becomes predominant at conditions close to ambient.

Equilibration during Core Formation

Simulations of molten pyrolite in contact with liquid iron at conditions along the mantle adiabat, show that during equilibration they remain two separate entities though they exchange a certain amount of atoms (Fig. 2a). In particular Si, and in a lesser extent O, exit the silicate melt, and penetrate into the iron. The presence of Si and O in the metallic melt ensure a realistic description of the two melts, which were in contact during the core formation process. Further chemical reactions occur at the interface, with the iron mixed with the silicate atoms. But the chemistries of the bulk of the two slabs are remarkably conserved throughout the simulations. This is a clear indication of the separation of the iron droplets during the process of core formation.

For each simulation, we consider all the snapshots after thermalisation. Then we define number density (ND) profiles along a given axis as the number of atoms of a certain type present at a given height along that axis. This is done for each snapshot. Then the number densities are summed up, averaged and normalised to the total number of snapshots in the simulation to provide concentrations. We chose the direction perpendicular to the interface to perform the ND analysis; we illustrate the chemical affinities of the different atoms of the simulations in Figure 2b. At conditions close to the MO adiabat, iron and oxygen ND profiles show regions with flat and non-overlapping high density values, corresponding respectively to homogeneous core and pyrolitic slabs. The He ND curves have high flat regions superposed to the pyrolite slab, and low flat regions, corresponding to the iron slab. This shows a clear preference for He partitioning into the MO. We observe the same trend even for different initial configurations (He on the interface, inside the pyrolite slab, or inside the iron slab) and for larger concentrations (8 He atoms) (Figs. S-2 to S-5). The preference of He for the silicate melt is so strong that over a simulation of up to 60 picoseconds, *i.e.* 60,000 successive steps, with 4 or 8 He atoms, only in a few hundred instances do He atoms lie in the metallic melt, the rest of the time being in the silicate part. Moreover, in simulations that start with He placed in the middle of the metallic slab, He leaves the molten iron over time scales on the order of hundreds of femtoseconds, and is further trapped in the pyrolite melt. Even at temperatures much higher than the adiabat, He partitions mainly into the pyrolite fraction at pressures in the 80–240 GPa range (Fig. S-3).

The ratio between ND of the same atomic type in pyrolite and iron melts yields the chemical partitioning, hereby $D_{\mathrm{He}}^{\mathrm{Fe/Silicate}}$. Our results (Fig. 3) indicate that He is lithophile at all MO conditions. We obtain $D_{\mathrm{He}}^{\mathrm{Fe/Silicate}} = 3.4 \times 10^{-4}$ close to the shallow MO conditions (3 GPa and 2000 K), increasing to

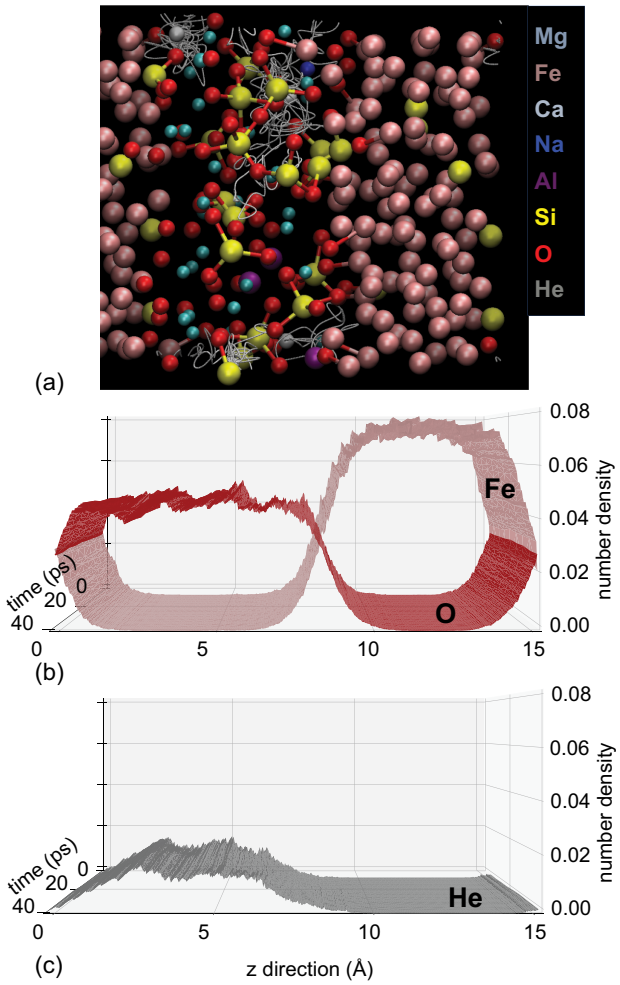

Figure 2 **(a)** Snapshot of the contact simulations between liquid pyrolite and molten iron (2000 K, 3 GPa). The trajectories of He atoms are represented over 8 ps of simulation, with grey ribbons. **(b)** ND profiles of Fe and O separate the two melts. The interface is highly localised and characterised by steep gradients of the Fe and O concentration. **(c)** ND profiles for He, which lie almost entirely in the silicate melt, as observed also in the trajectories of the individual atoms.

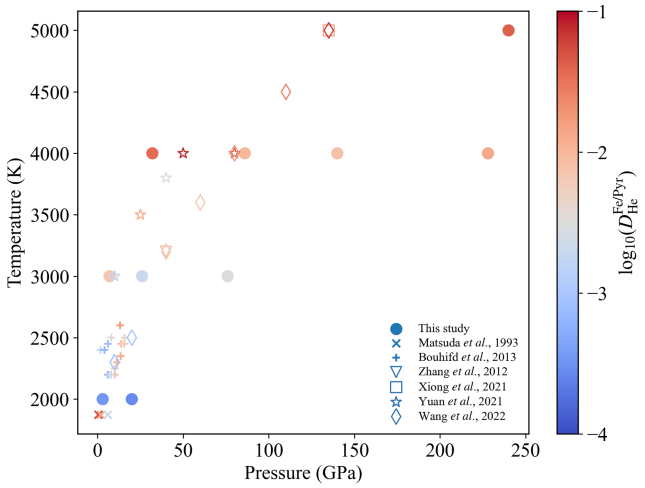

Figure 3 Metal/silicate He partition coefficients. Previous experimental data are shown with crosses and previous computed results by open symbols. Present study is plotted with solid symbols. The affinity of He for the silicate melt decreases along the mantle adiabat by about two orders of magnitude between the top and the bottom of the MO.

1.0×10^{-2} close to the core-mantle boundary (140 GPa and 4000 K) and up to 4.2×10^{-2} at higher pressures and temperatures (240 GPa and 5000 K). While partition coefficients change with pressure, the main governing factor is temperature (Yuan and Steinle-Neumann, 2021). Increasing the temperature by 2000 K, approximately the difference between the surface and the bottom of the MO, decreases the partitioning by two orders of magnitude.

Experiments at realistic thermodynamic conditions are extremely difficult, because of the volatility of the noble gases and the small sample volumes produced for chemical analysis. Only few experimental studies exist (Matsuda *et al.*, 1993; Bouhifd *et al.*, 2013), but they cover a small *P*-*T* range. Recent *ab initio* molecular dynamics studies of He partitioning between molten $MgSiO_3$ and Fe (Xiong *et al.*, 2021; Yuan and Steinle-Neumann, 2021; Li *et al.*, 2022; Wang *et al.*, 2022) show that $D_{He}^{Fe/Silicate}$ is insensitive to pressure. $MgSiO_3$ values at 80 GPa are one order of magnitude smaller than pyrolite, probably because of the simplified chemistries. Simulations of partitioning between molten $MgSiO_3$ and liquid Fe-O alloys are closer to our results (Yuan and Steinle-Neumann, 2021), most probably because of the presence of O in the liquid core. This comparison shows that while He must have different affinities to different silicate melts, the exsolution of He from the liquid iron, which might be enhanced by the presence of light elements, is the most important factor acting on the core-mantle partitioning of noble gases during the process of core formation.

Conclusions

The bulk of the Earth's primordial noble gas content is acquired during the main accretion stage. Primordial He originates from either the early ingassing of solar nebula (Olson and Sharp, 2022) or accreting chondritic material irradiated by the solar wind (Moreira and Charnoz, 2016). Considering the short lifetime of the solar nebula (~3 Myr; Borlina *et al.*, 2022), He should originate mostly from solid accretion. Partial loss during giant impacts, and later enrichment by accreted materials slightly altered the initial concentration (Péron *et al.*, 2018).

During accretion, the integrity of the incoming planetesimals and meteorites is lost. Their silicate parts mix and disperse in the MO, while their cores may turn into small droplets inside the MO (Ichikawa *et al.*, 2010; Kendall and Melosh, 2016). Centimetre or millimetre-sized droplets totally equilibrate in the MO within a few tens of metres (Rubie *et al.*, 2003), and based on our partitioning results, lose 99.999 % of their initial He. As such, they arrive into the core heavily depleted in He. Larger droplets (yet smaller than the MO thickness) break during descent to smaller centimetre-sized stable droplets, which attain equilibrium before reaching the bottom of MO (Samuel, 2012). This suggests that He equilibration occurs earlier in the MO, at shallow conditions with lower $D_{He}^{Fe/Silicate}$, in contrast to previous assumptions of equilibration at the core mantle boundary (Xiong *et al.*, 2021; Yuan and Steinle-Neumann, 2021; Wang *et al.*, 2022).

As a result of the large and giant impacts of the accretion (Canup, 2004; Ćuk and Stewart, 2012), the MO was covered by a thick and hot silicate atmosphere. The top of the MO witnessed temperatures higher than 2000 K and pressures of at least several kilobars. According to our simulations, at these conditions, He remains mostly dissolved in the MO (Fig. 4a). Later, after

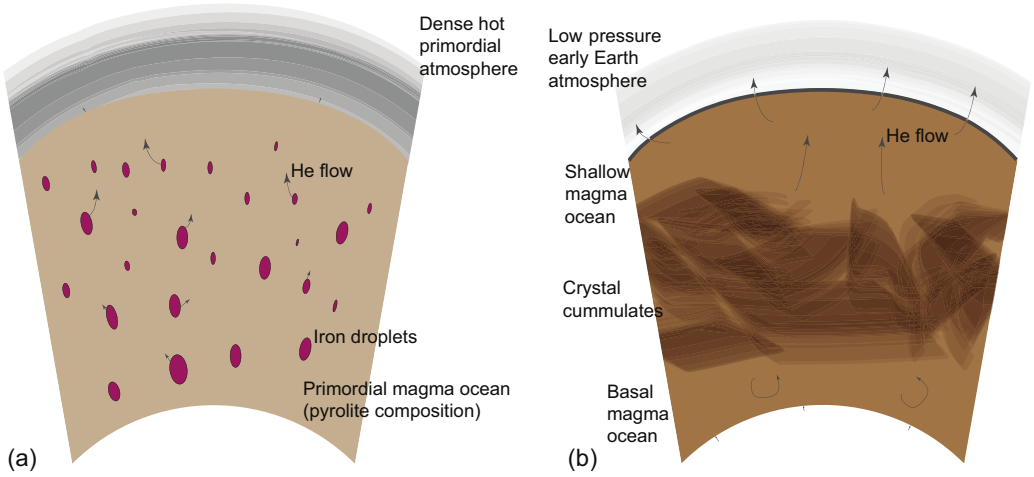

Figure 4 Cartoon representation of He fluxes (arrows) during core formation through the MO model. There is a strong initial transfer of He from the iron droplets to the silicate magma. **(a)** The hot, dense atmosphere prevents degassing and escape of He. **(b)** With cooling and formation of a crystal layer at mid-depths, He is trapped in the basal MO, while the shallow MO undergoes massive evaporation to the secondary colder and less dense atmosphere.

decreasing pressure, a large amount of He could have been degassed. The degassing would dominate the shallow MO, until a protective lid forms relatively late, at around 500–800 million years (Monteux *et al.*, 2020) (Fig. 4b). However, deep in the mantle, a chemically and thermally isolated basal MO may survive up to 2.5 Gyr (Blanc *et al.*, 2020). As it crystallised, its load of incompatible elements concentrated, which were eventually captured in the last rocks forming at the base of the mantle. Long lifetime of basal MO also implies long chemical exchange with the core, which continually lost its He into the molten silicate (Fig. 4b).

Assuming that Earth is mainly accreted from enstatite chondrites with 1.33×10^{-8} mol/kg of ^{3}He (Patzer and Schultz, 2001), and using calculated $D_{\mathrm{He}}^{\mathrm{Fe/Silicate}}$ of $\sim 10^{-3}$ at 3000 K (temperature at which iron silicate starts to segregate), the estimated abundance of ^{3}He in the Earth's core can be on the order of 4.0×10^{-11} mol/kg. Higher values might be possible, based on alternate accretion scenarios (Olson and Sharp, 2022). Nevertheless, our value is higher than previous estimations from Fe-$MgSiO_3$, but at least one order of magnitude lower than that stemming from the Fe-O alloy-$MgSiO_3$ system (Yuan and Steinle-Neumann, 2021). These numbers are also about one order of magnitude smaller than previous experimental estimates (10^{-11}–10^{-10}; Bouhifd *et al.*, 2013). Combining the primordial ^{3}He concentration in the core with the amount of ^{4}He produced from the U and Th budget of the core over 4.5 Ga (10^{-6} mol/kg; Yuan and Steinle-Neumann, 2021), the current ^{3}He/^{4}He in the core would be about 28 Ra, far lower than highest isotopic signature (50 Ra). This is a higher limit estimation for ^{3}He abundance without taking into account He degassing during impacts. This suggests that the core cannot play a significant role as a reservoir of high primordial helium. It is then apparent that the source of rocks like OIBs, with high ^{3}He/^{4}He ratios, taps into a geochemical reservoir which should be somewhere at the bottom of the mantle, consistent with conclusions derived from Ne partitioning (Li *et al.*, 2022).

Acknowledgments

This work was supported by the Research Council of Norway through its Centres of Excellence funding scheme, project number 223272, and through project HIDDEN 325567. RC acknowledges support from the European Research Council under EU Horizon 2020 research and innovation programme (grant agreement 681818 – IMPACT), and for access to supercomputing facilities *via* eDARI stl2816 grants, PRACE RA4947 and RA0046 grants, and Uninet2 NN9697K grant.

Editor: Anat Shahar

Additional Information

Supplementary Information accompanies this letter at https://www.geochemicalperspectivesletters.org/article2314.

Cite this letter as: Ozgurel, O., Caracas, R. (2023) The magma ocean was a huge helium reservoir in the early Earth. *Geochem. Persp. Let.* 25, 46–50. https://doi.org/10.7185/geochemlet.2314

References

Blanc, N.A., Stegman, D.R., Ziegler, L.B. (2020) Thermal and magnetic evolution of a crystallizing basal magma ocean in Earth's mantle. *Earth and Planetary Science Letters* 534, 116085. https://doi.org/10.1016/j.epsl.2020.116085

Borlina, C.S., Weiss, B.P., Bryson, J.F.J., Armitage, P.J. (2022) Lifetime of the Outer Solar System Nebula From Carbonaceous Chondrites. *Journal of Geophysical Research: Planets* 127, e2021JE007139. https://doi.org/10.1029/2021JE007139

Bouhifd, M.A., Jephcoat, A.P., Heber, V.S., Kelley, S.P. (2013) Helium in Earth's early core. *Nature Geoscience* 6, 982–986. https://doi.org/10.1038/ngeo1959

Canup, R.M. (2004) Simulations of a late lunar-forming impact. *Icarus* 168, 433–456. https://doi.org/10.1016/j.icarus.2003.09.028

Class, C., Goldstein, S.L. (2005) Evolution of helium isotopes in the Earth's mantle. *Nature* 436, 1107–1112. https://doi.org/10.1038/nature03930

Ćuk, M., Stewart, S.T. (2012) Making the Moon from a Fast-Spinning Earth: A Giant Impact Followed by Resonant Despinning. *Science* 338, 1047–1052. https://doi.org/10.1126/science.1225542

Farley, K.A., Natland, J.H., Craig, H. (1992) Binary mixing of enriched and undegassed (primitive?) mantle components (He, Sr, Nd, Pb) in Samoan lavas. *Earth and Planetary Science Letters* 111, 183–199. https://doi.org/10.1016/0012-821X(92)90178-X

Ichikawa, H., Labrosse, S., Kurita, K. (2010) Direct numerical simulation of an iron rain in the magma ocean. *Journal of Geophysical Research: Solid Earth* 115, B01404. https://doi.org/10.1029/2009JB006427

Jackson, M.G., Carlson, R.W. (2011) An ancient recipe for flood-basalt genesis. *Nature* 476, 316–319. https://doi.org/10.1038/nature10326

Jackson, M.G., Konter, J.G., Becker, T.W. (2017) Primordial helium entrained by the hottest mantle plumes. *Nature* 542, 340–343. https://doi.org/10.1038/nature21023

Kendall, J.D., Melosh, H.J. (2016) Differentiated planetesimal impacts into a terrestrial magma ocean: Fate of the iron core. *Earth and Planetary Science Letters* 448, 24–33. https://doi.org/10.1016/j.epsl.2016.05.012

Kurz, M.D., Geist, D. (1999) Dynamics of the Galapagos hotspot from helium isotope geochemistry. *Geochimica et Cosmochimica Acta* 63, 4139–4156. https://doi.org/10.1016/S0016-7037(99)00314-2

Li, Y., Vočadlo, L., Ballentine, C., Brodholt, J.P. (2022) Primitive noble gases sampled from ocean island basalts cannot be from the Earth's core. *Nature Communications* 13, 3770. https://doi.org/10.1038/s41467-022-31588-7

Marty, B. (2012) The origins and concentrations of water, carbon, nitrogen and noble gases on Earth. *Earth and Planetary Science Letters* 313–314, 56–66. https://doi.org/10.1016/j.epsl.2011.10.040

Matsuda, J., Sudo, M., Ozima, M., Ito, K., Ohtaka, O., Ito, E. (1993) Noble Gas Partitioning Between Metal and Silicate Under High Pressures. *Science* 259, 788–790. https://doi.org/10.1126/science.259.5096.788

McDonough, W.F., Sun, S.-s. (1995) The composition of the Earth. *Chemical Geology* 120, 223–253. https://doi.org/10.1016/0009-2541(94)00140-4

Monteux, J., Andrault, D., Guitreau, M., Samuel, H., Demouchy, S. (2020) A mushy Earth's mantle for more than 500 Myr after the magma ocean solidification. *Geophysical Journal International* 221, 1165–1181. https://doi.org/10.1093/gji/ggaa064

Moreira, M. (2013) Noble Gas Constraints on the Origin and Evolution of Earth's Volatiles. *Geochemical Perspectives* 2, 229–403. https://doi.org/10.7185/geochempersp.2.2

Moreira, M., Charnoz, S. (2016) The origin of the neon isotopes in chondrites and on Earth. *Earth and Planetary Science Letters* 433, 249–256. https://doi.org/10.1016/j.epsl.2015.11.002

Mukhopadhyay, S., Parai, R. (2019) Noble Gases: A Record of Earth's Evolution and Mantle Dynamics. *Annual Review of Earth and Planetary Sciences* 47, 389–419. https://doi.org/10.1146/annurev-earth-053018-060238

Olson, P.L., Sharp, Z.D. (2022) Primordial Helium-3 Exchange Between Earth's Core and Mantle. *Geochemistry, Geophysics, Geosystems* 23, e2021GC009985. https://doi.org/10.1029/2021GC009985

Patzer, A., Schultz, L. (2001) Noble gases in enstatite chondrites I: Exposure ages, pairing, and weathering effects. *Meteoritics & Planetary Science* 36, 947–961. https://doi.org/10.1111/j.1945-5100.2001.tb01932.x

Péron, S., Moreira, M., Agranier, A. (2018) Origin of Light Noble Gases (He, Ne, and Ar) on Earth: A Review. *Geochemistry, Geophysics, Geosystems* 19, 979–996. https://doi.org/10.1002/2017GC007388

Rubie, D.C., Melosh, H.J., Reid, J.E., Liebske, C., Righter, K. (2003) Mechanisms of metal–silicate equilibration in the terrestrial magma ocean. *Earth and Planetary Science Letters* 205, 239–255. https://doi.org/10.1016/S0012-821X(02)01044-0

Samuel, H. (2012) A re-evaluation of metal diapir breakup and equilibration in terrestrial magma oceans. *Earth and Planetary Science Letters* 313–314, 105–114. https://doi.org/10.1016/j.epsl.2011.11.001

Solomatova, N.V., Caracas, R. (2021) Genesis of a CO_2-rich and H_2O-depleted atmosphere from Earth's early global magma ocean. *Science Advances* 7, eabj0406. https://doi.org/10.1126/sciadv.abj0406

Stuart, F.M., Lass-Evans, S., Godfrey Fitton, J., Ellam, R.M. (2003) High $^3He/^4He$ ratios in picritic basalts from Baffin Island and the role of a mixed reservoir in mantle plumes. *Nature* 424, 57–59. https://doi.org/10.1038/nature01711

Tolstikhin, I., Hofmann, A.W. (2005) Early crust on top of the Earth's core. *Physics of the Earth and Planetary Interiors* 148, 109–130. https://doi.org/10.1016/j.pepi.2004.05.011

Trieloff, M., Kunz, J. (2005) Isotope systematics of noble gases in the Earth's mantle: possible sources of primordial isotopes and implications for mantle structure. *Physics of the Earth and Planetary Interiors* 148, 13–38. https://doi.org/10.1016/j.pepi.2004.07.007

Wang, K., Lu, X., Liu, X., Zhou, M., Yin, K. (2022) Partitioning of noble gases (He, Ne, Ar, Kr, Xe) during Earth's core segregation: A possible core reservoir for primordial noble gases. *Geochimica et Cosmochimica Acta* 321, 329–342. https://doi.org/10.1016/j.gca.2022.01.009

Xiong, Z., Tsuchiya, T., Van Orman, J.A. (2021) Helium and Argon Partitioning Between Liquid Iron and Silicate Melt at High Pressure. *Geophysical Research Letters* 48, e2020GL090769. https://doi.org/10.1029/2020GL090769

Yuan, L., Steinle-Neumann, G. (2021) The Helium Elemental and Isotopic Compositions of the Earth's Core Based on Ab Initio Simulations. *Journal of Geophysical Research: Solid Earth* 126, e2021JB023106. https://doi.org/10.1029/2021JB023106

Geochemical Perspectives Letters

The magma ocean was a huge helium reservoir in the early Earth

O. Ozgurel, R. Caracas

Supplementary Information

The Supplementary Information includes:

- Computational Details
- Figures S-1 to S-6
- Table S-1
- Supplementary Information References

Computational Details

We performed *ab initio* molecular dynamics simulations based on density functional theory as implemented in the Vienna Ab initio Simulation Package (VASP; Kresse and Hafner, 1993; Kresse and Furthmüller, 1996). A plane wave basis set is used to represent the electron density. The core electrons are kept frozen and replaced by pseudo-potentials generated by the plane augmented wave method (PAW; Blöchl, 1994; Kresse and Joubert, 1999). We used the generalised gradient approximation (GGA) in the form of PBE exchange-correlation functional (Perdew *et al*., 1996). The simulations are spin-polarised at all conditions. The kinetic energy cut-off for the planewave basis set and the augmentation charges inside the PAW spheres were set to 550 and 850 eV, respectively. Fermi smearing was used for all calculations, setting the smearing width according to the simulation temperature.

The molecular dynamics calculations have been performed within a NVT canonical ensemble with a Nosé-Hoover thermostat (Nosé, 1984; Hoover, 1985). The cubic simulation cell is composed of two melts in contact, with starting compositions corresponding to pyrolite, *i.e.* the bulk silicate Earth (McDonough and Sun, 1995) and pure iron. Pyrolite represents the magma ocean (MO), with initial stoichiometry $NaCa_2Fe_4Mg_{30}Al_3Si_{24}O_{89}$ (153 atoms; Solomatova and Caracas, 2019), whereas the core was modelled as molten iron with 108 atoms. The two melts are arranged in contact, in slabs perpendicular to the z direction. The Brillouin zone was sampled at the Gamma point.

To calculate volatilisation, we expand the volumes of the He-bearing pyrolite melts until we reach the liquid-vapor dome. Then we build the interatomic connectivity graph at each timestep. That yields a bimodal distribution, with isolated atoms and molecules and large polymers. The former constitutes the gas phase and the latter the liquid phase. To calculate partition coefficients of He between core and MO, we put in contact

pyrolite and iron melt. Then we introduce 4 He atoms on the interface between the two slabs. Additionally, a set of simulations with 8 He atoms and different starting configurations (inside the iron slab and inside the pyrolite slab) were conducted to decrease as much as possible configurational bias. We performed the simulations covering the whole range of MO adiabats at 2000–5000 K and 3–240 GPa. Simulations at 5000 K and at pressures lower than 240 GPa were discarded as the two slabs mix. Hence the setup of the simulations with two melts in contact has two advantages over the thermodynamic integration method: the equilibration of the two melts allows for an exchange of atoms, and the conditions at which the two melts completely mix are discarded, as unphysical for computing proper partitioning coefficients. The total simulation time at each temperature and pressure is at least 20 ps with a time-step of 1–4 fs, depending on the system.

The area under the partial number density curves is directly related to the amount of atoms present within the slab and can be used to calculate their concentrations, assuming that trajectories are long enough to sample the He migration in two-melt system adequately. In our simulations the average distance travelled by the He atoms is at least the full width of the slabs, thus giving them the probabilistic time to sample the two parts of the simulation box. We calculated the concentration of He within the bulk parts of the iron and the pyrolite melts and neglecting the interface region on purpose as it does not necessarily represent equilibrium. The ratio of these concentrations gives the iron to pyrolite partition coefficient of He.

To study He vaporisation from the MO, we introduced 2 or 8 He atoms to the pyrolite melt and conducted simulations at 3000 K, 4000 K and 5000 K. We consider densities ranging from 1.1–2.0 g/cm^3. Though the He concentrations are larger than the actual values, this choice is dictated by limitations in computations, and ensures higher reliability of our results. We employed the same approach as in the previous vaporisation study (Solomatova and Caracas, 2021): early atmosphere conditions are introduced to the system as a given pressure and temperature acting on magma ocean without considering the atmospheric molecular composition. Throughout the simulation, He is able to continuously trade place between the void space as vapor molecules and the bulk of the silicate melts, as dissolved in the liquid. To distinguish between the two configurations, we perform a full speciation analysis based on the connectivity matrix between the atoms. For this, bond distances were determined from the radial distribution function. The first peak in the radial distribution function approximates the average bond length, whereas the first minimum in the radial distribution function corresponds to the radius of the first coordination sphere of atom (Fig. S-1). This value is used as a geometric cut-off length to consider two atoms bonded and were used in the volatility of He in the pyrolite melts with the speciation module of the Universal Molecular Dynamics package (Caracas *et al*., 2021). Vaporised He is defined as a component not bound to the interconnected silicate melt polymer. The proportion of species in the vapor and melt phases is calculated from an average over the entire simulation. The addition of further volatiles in the MO can enhance degassing of He, by decreasing the density of the melt, and promoting the opening of gas bubbles. On the other hand, the presence of the same other volatiles in the gas bubbles raises the gas pressure which prevents He from evaporating. Consequently, there are two possible competing effects, and they need to be thoroughly studied on a case-by-case basis. We prefer not to adventure here into a too speculative discussions, and rather wait for more experimental data or computational results.

Supplementary Figures

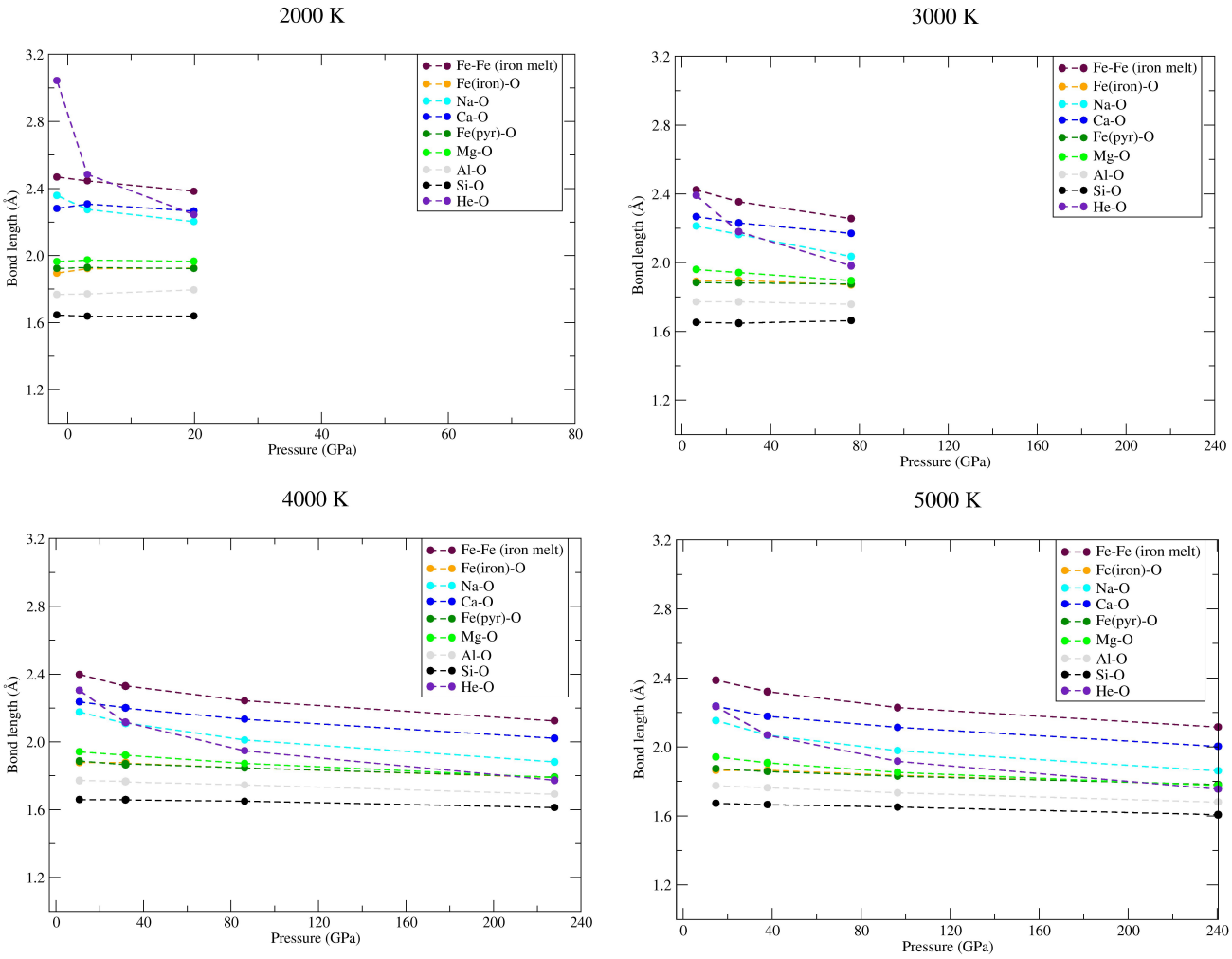

Figure S-1 Average bond lengths as a function of pressure, as approximated by the position of the first peak of the corresponding cation-oxygen radial distribution functions.

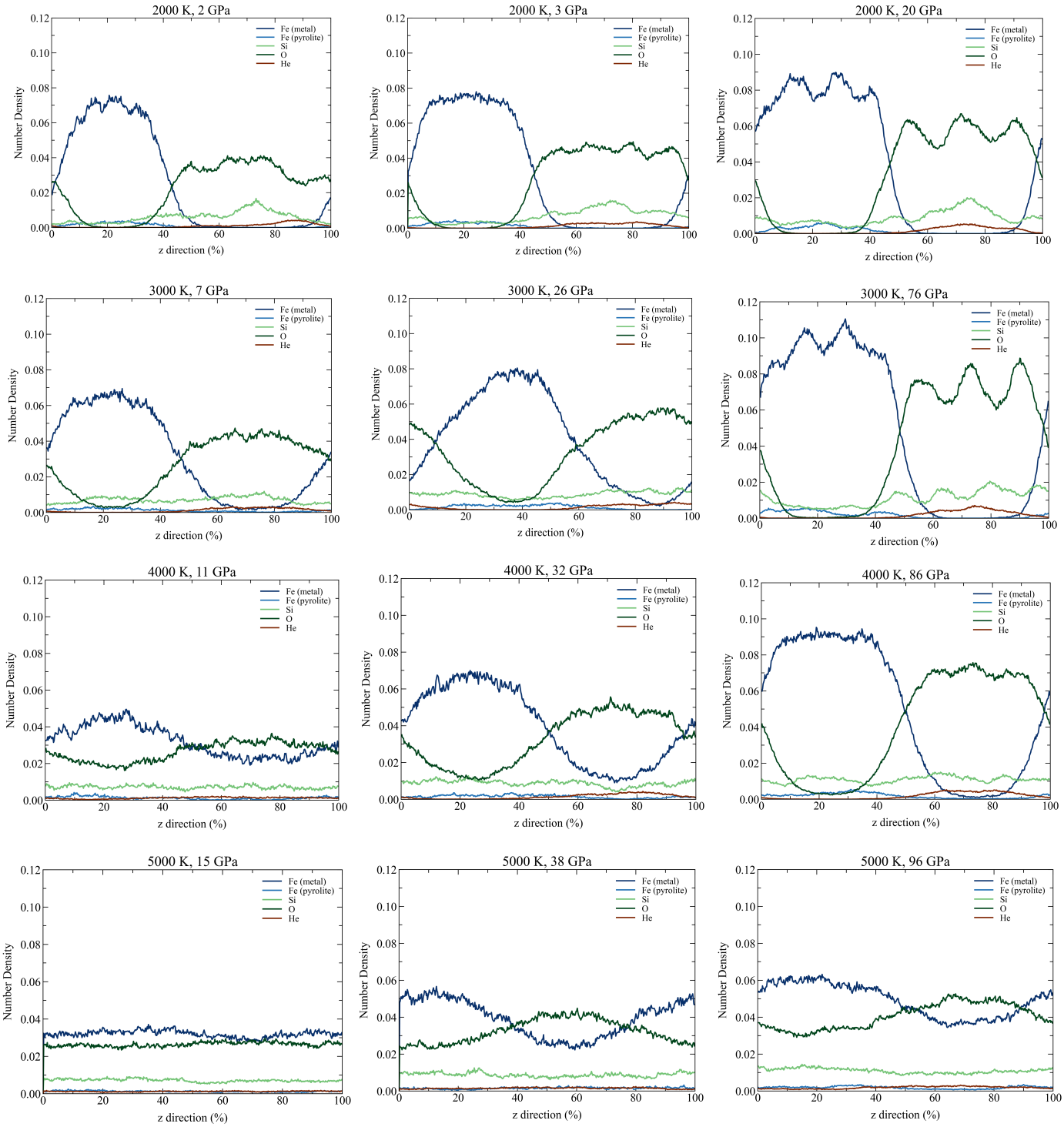

Figure S-2 Number density profiles along the *z* direction for Fe (both in metal and pyrolite), Si, O and He. 4 He atoms are introduced to the systems on the iron/pyrolite interface. From top to bottom, the temperature of the system is 2000 K, 3000 K, 4000 K and 5000 K, respectively.

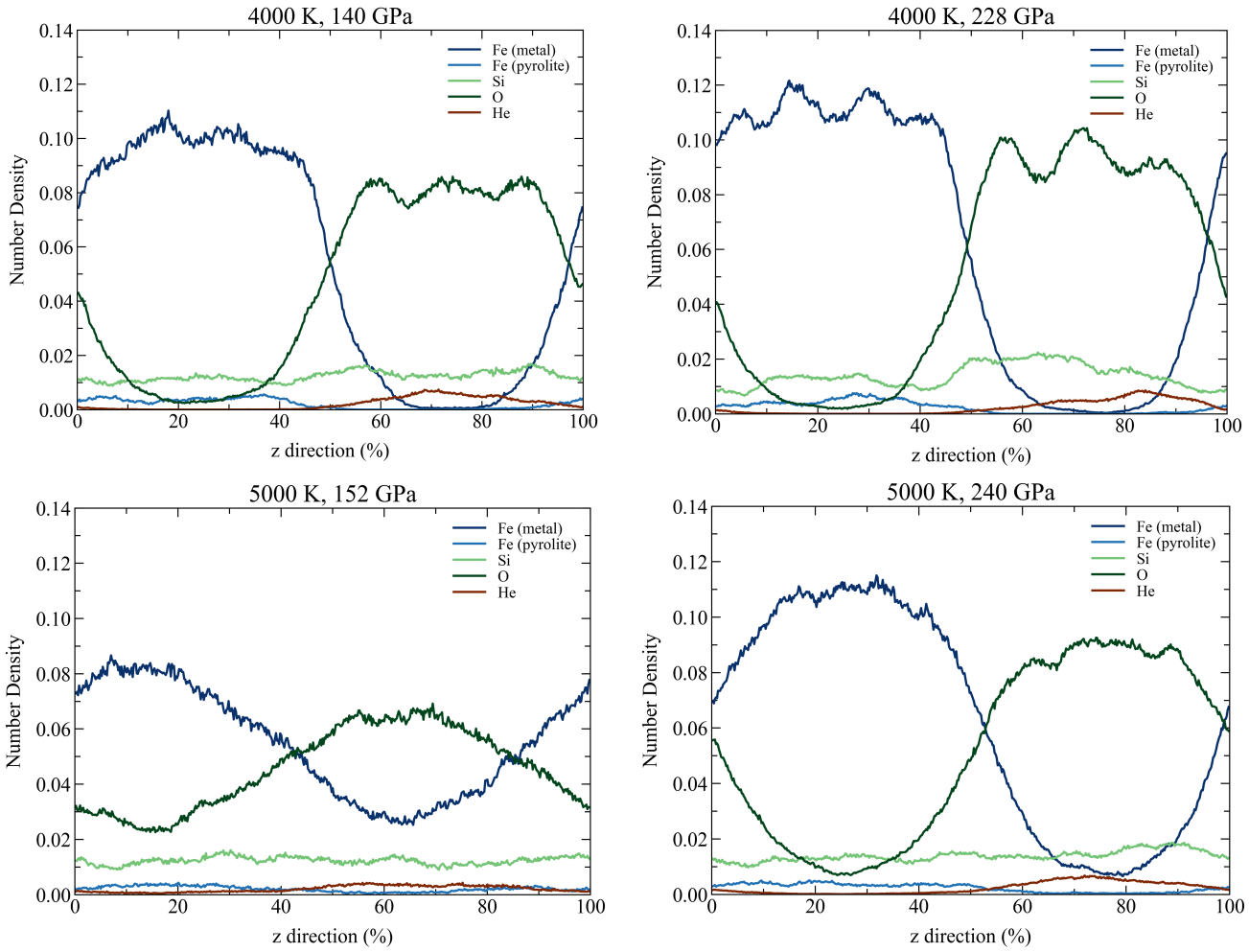

Figure S-3 Number density profiles along the *z* direction for Fe (both in metal and pyrolite), Si, O and He at high pressures (>100 GPa) and 4000 K or 5000 K. Four He atoms are introduced to the systems inside the iron slab. Four He atoms are introduced to the systems on the iron/pyrolite interface.

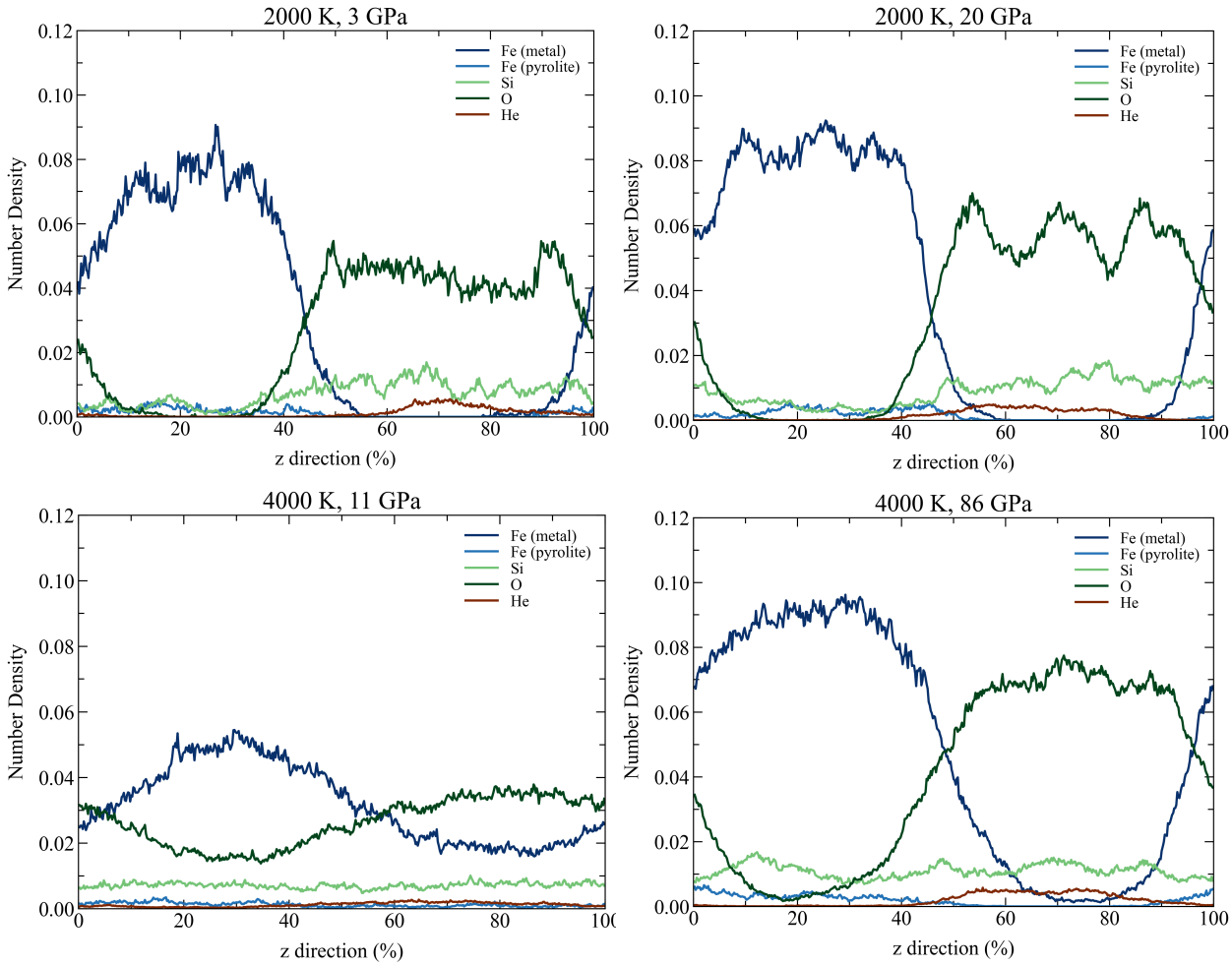

Figure S-4 Number density profiles along the *z* direction for Fe (both in metal and pyrolite), Si, O and He. Four He atoms are introduced to the systems inside the iron slab.

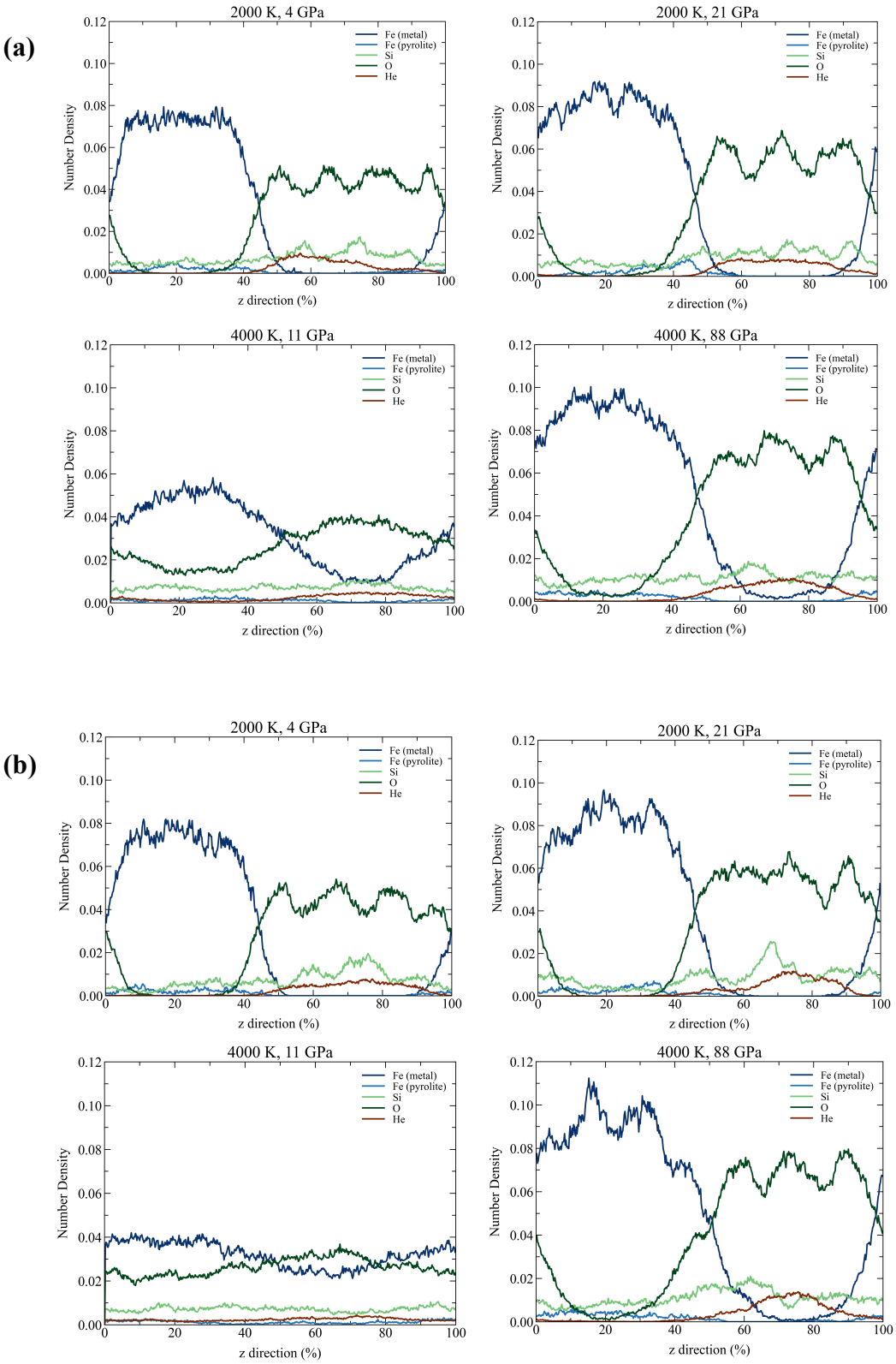

Figure S-5 Number density profiles along the *z* direction for Fe (both in metal and pyrolite), Si, O and He. Eight He atoms are introduced in the simulations inside **(a)** the pyrolite slab and **(b)** the iron slab.

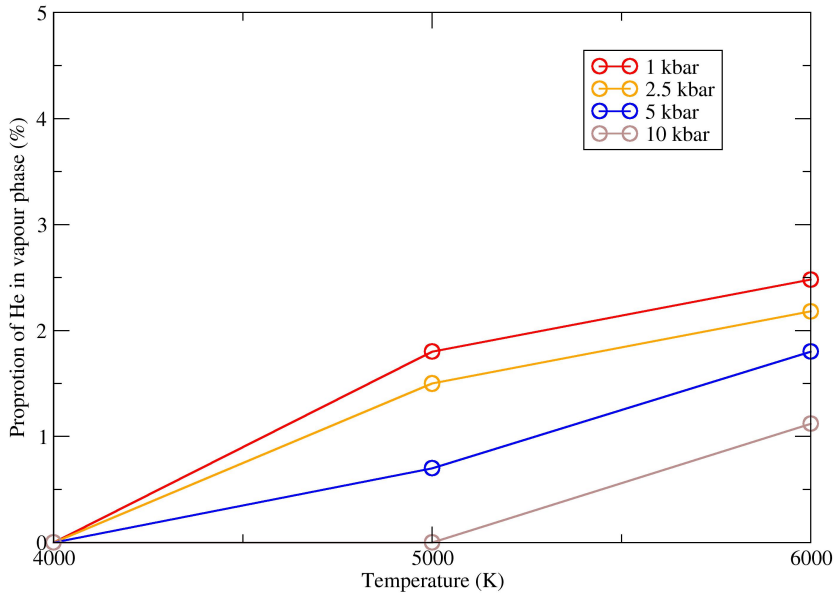

Figure S-6 Proportion of vaporised He as a function of temperature along isobars of 1 to 10 kbar.

Supplementary Table

Table S-1 Zero-pressure density (ρ_0), zero-pressure bulk modulus (K_0) and the first derivative of the bulk modulus (K') at 4000–6000 K, obtained from fitting a third-order Birch Murnaghan (BM) equation of state to the pressure-density data.

T (K)	ρ_0 (g/cm^3)	K_0 (GPa)	K'
4000	2.04	11.1	5.5
5000	1.79	6.6	5.9
6000	1.64	6.1	5.4

Supplementary Information References

Blöchl, P.E. (1994) Projector augmented-wave method. *Physical Review B* 50, 17953. https://doi.org/10.1103/PhysRevB.50.17953

Caracas, R., Kobsch, A., Solomatova, N.V., Li, Z., Soubiran, F., Hernandez, J.-A. (2021) Analyzing Melts and Fluids from Ab Initio Molecular Dynamics Simulations with the UMD Package. *Journal of Visualized Experiments* 175, e61534. https://doi.org/10.3791/61534

Hoover, W.G. (1985) Canonical dynamics: Equilibrium phase-space distributions. *Physical Review A* 31, 1695. https://doi.org/10.1103/PhysRevA.31.1695

Kresse, G., Hafner, J. (1993) *Ab initio* molecular dynamics for liquid metals. *Physical Review B* 47, 558. https://doi.org/10.1103/PhysRevB.47.558

Kresse, G., Furthmüller, J. (1996) Efficient iterative schemes for *ab initio* total-energy calculations using a plane-wave basis set. *Physical Review B* 54, 11169. https://doi.org/10.1103/PhysRevB.54.11169

Kresse, G., Joubert, D. (1999) From ultrasoft pseudopotentials to the projector augmented-wave method. *Physical Review B* 59, 1758. https://doi.org/10.1103/PhysRevB.59.1758

McDonough, W.F., Sun, S.-s. (1995) The composition of the Earth. *Chemical Geology* 120, 223–253. https://doi.org/10.1016/0009-2541(94)00140-4

Nosé, S. (1984) A unified formulation of the constant temperature molecular dynamics methods. *The Journal of Chemical Physics* 81, 511–519. https://doi.org/10.1063/1.447334

Perdew, J.P., Burke, K., Wang, Y. (1996) Generalized gradient approximation for the exchange-correlation hole of a many-electron system. *Physical Review B* 54, 16533. https://doi.org/10.1103/PhysRevB.54.16533

Solomatova, N.V., Caracas, R. (2019) Pressure-Induced Coordination Changes in a Pyrolitic Silicate Melt From Ab Initio Molecular Dynamics Simulations. *Journal of Geophysical Research: Solid Earth* 124, 11232–11250. https://doi.org/10.1029/2019JB018238

Solomatova, N.V., Caracas, R. (2021) Genesis of a CO_2-rich and H_2O-depleted atmosphere from Earth's early global magma ocean. *Science Advances* 7, eabj0406. https://doi.org/10.1126/sciadv.abj0406